Bioactive Materials 6 (2021) 3999–4013

Contents lists available at ScienceDirect

Bioactive Materials

journal homepage: www.sciencedirect.com/journal/bioactive-materials

Biodegradable ZnLiCa ternary alloys for critical-sized bone defect regeneration at load-bearing sites: *In vitro* and *in vivo* studies

Zechuan Zhang [a,1], Bo Jia [b,c,1], Hongtao Yang [a,d], Yu Han [b], Qiang Wu [b], Kerong Dai [b,**], Yufeng Zheng [a,*]

[a] School of Materials Science and Engineering, Peking University, Beijing, 100871, China
[b] Department of Orthopedic Surgery, Shanghai Key Laboratory of Orthopedic Implants, Shanghai Ninth People's Hospital, Shanghai Jiao Tong University, School of Medicine, Shanghai, 200011, China
[c] Department of Orthopedics, Shanghai General Hospital, Shanghai Jiao Tong University School of Medicine, Shanghai, 200080, China
[d] School of Medical Science and Engineering, Beihang University, Beijing, 100191, China

ARTICLE INFO

Keywords:
ZnLiCa alloys
Biodegradable metal
Critical-sized bone defect
Orthopedics
Porous scaffold
In vivo

ABSTRACT

A novel biodegradable metal system, ZnLiCa ternary alloys, were systematically investigated both *in vitro* and *in vivo*. The ultimate tensile strength (UTS) of Zn0.8Li0.1Ca alloy reached 567.60 ± 9.56 MPa, which is comparable to pure Ti, one of the most common material used in orthopedics. The elongation of Zn0.8Li0.1Ca is 27.82 ± 18.35%, which is the highest among the ZnLiCa alloys. The *in vitro* degradation rate of Zn0.8Li0.1Ca alloy in simulated body fluid (SBF) showed significant acceleration than that of pure Zn. CCK-8 tests and hemocompatibility tests manifested that ZnLiCa alloys exhibit good biocompatibility. Real-time PCR showed that Zn0.8Li0.1Ca alloy successfully stimulated the expressions of osteogenesis-related *genes* (ALP, COL-1, OCN and Runx-2), especially the OCN. An *in vivo* implantation was conducted in the radius of New Zealand rabbits for 24 weeks, aiming to treat the bone defects. The Micro-CT and histological evaluations proved that the regeneration of bone defect was faster within the Zn0.8Li0.1Ca alloy scaffold than the pure Ti scaffold. Zn0.8Li0.1Ca alloy showed great potential to be applied in orthopedics, especially in the load-bearing sites.

1. Introduction

Bone is a dynamic system which could maintain its homeostasis under small defects [1]. However, when the defects are larger than a critical-size [2,3], which are frequently caused by trauma, infection, tumors or other ailments [4], the bone might lose the ability to recover independently [5]. To address this problem, there are mainly two approaches nowadays —bone grafts and bone tissue engineering [6]. Bone grafts, including autografts, allografts and xenografts, are widely used in the treatment of bone defects [7]. However, several disadvantages, such as immune response, probability of diseases transmission, and donor shortage, have limited their applications greatly [8]. Hence, bone tissue engineering has been investigated as an alternative way to treat bone defects.

Generally speaking, there are mainly four types of materials used for bone tissue engineering, including polymers (natural or synthetic), bioactive ceramics, composites of polymers and ceramics and metallic materials [9]. Among these materials, polymers, ceramics and their composites often could not provide enough mechanical supports for the load-bearing positions [10]. Traditional metallic materials, like titanium, stainless steel or tantalum, could provide enough mechanical supports. However, their non-biodegradable properties render them cannot be fetched out after new bone has grown together with the implants, which would increase the suffering and burdens of patients [11]. Their long-term existence would also increase the risks of inflammation and infections. Thus, an ideal material for bone tissue engineering should provide enough mechanical supports, be biodegradable, and have good biocompatibility as well as osteogenic activity [6,12].

Peer review under responsibility of KeAi Communications Co., Ltd.
* Corresponding author. Department of Materials Science and Engineering, College of Engineering, Peking University, Beijing, 100871, China.
** Corresponding author. Department of Orthopedics, Ninth People's Hospital, Shanghai Jiao Tong University, School of Medicine, 639 Zhizaoju Road, Shanghai, 200011, China.
E-mail addresses: krdai@163.com (K. Dai), yfzheng@pku.edu.cn (Y. Zheng).
[1] These authors contributed equally to this work.

https://doi.org/10.1016/j.bioactmat.2021.03.045
Received 9 March 2021; Received in revised form 29 March 2021; Accepted 29 March 2021

Therefore, biodegradable metals, which could be biodegraded *in vivo* while assisting the tissue with healing, have been investigated as a promising candidate [13,14].

Zn-based biodegradable metals have been a hot topic in the research field since the last decade. Playing an indispensable role in the bone metabolism [15], element Zn contributes a lot to the bone remodeling by stimulating the osteoblasts while inhibiting the osteoclasts [16,17]. However, the mechanical properties of pure Zn is unsatisfactory [18,19]. To enhance the performance of Zn-based biodegradable metals, alloying elements, including Li [20,21], Mg [22–28], Ca [29,30], Sr [12,31], Cu [32–35], Ag [36–38], Mn [39–42] and Fe [43,44], were introduced into the system. Among these researches, element Li have brought the most significant improvement in mechanical strength [45]. However, the biocompatibility of Zn–Li alloys were still not ideal [46,47]. Besides, although the ductility of Zn–Li alloys are generally good [48]. For as-rolled Zn-0.8Li alloy, the elongation can be around 75% [49]. The strength-ductility compromise effect is significant. For as-rolled Zn-0.7Li alloy, the strength can be higher than 560 MPa, while the elongation is merely 2.5% [50]. The comprehensive mechanical properties of Zn–Li alloys need further improvement.

Ca is the most common mineral element of human body and a critical component of the bone [51]. Also, Ca is an important component of many biomaterials, such as hydroxyapatite (HA) [52,53], tricalcium phosphate (TCP) [54,55], and silicates [56,57]. Moreover, Ca has been widely used as an alloying element in biodegradable metals, such as Mg-Ca [58,59], Zn-Ca [29,30], Mg-Zn-Ca [60–62], etc. Previous studies have shown that Ca could bring improvements in the biocompatibility and mechanical properties of the biodegradable metals. Therefore, element Ca was selected as a tertiary alloying element to be added in the Zn–Li alloys.

In this study, a novel ZnLiCa biodegradable metal system was prepared. And their mechanical properties, *in vitro* degradation properties and cytotoxicity were carefully studied. Porous biodegradable scaffolds fabricated of Zn0.8Li0.1Ca alloy, were implanted in a New Zealand rabbit model to treat radial bone bone defects, and pure Ti was selected as a control group. Multiple methods, including histological evaluations, micro-CT, and energy dispersive spectrometer (EDS) were employed to evaluate the bone repair effects.

2. Materials and methods

2.1. Materials preparation

High-purity Zn(99.99%), Li(99.95%) and Ca(99.99%) were used to prepare ZnLiCa alloys and the control groups (pure Zn and Zn0.8Li). The alloys' compositions were listed in Table 1. The pure metals were firstly melt at 540 °C and then cast into cylindrical shape. Then the as-cast alloys were extruded into bars (temperature: 210 °C, extrusion ratio: 16). The as-extruded materials were used to conduct subsequent experiments. Disk-like specimens (Φ10 × 2 mm^3) were wire-cut from the bars perpendicular to the extrusion direction. Before usages, all the specimens were mechanically polished, rinsed with ethanol and acetone, and dried in the air.

Table 1
Analyzed compositions of the studied ZnLiCa ternary alloys and control group.

Nominal Composition (wt.%)	Analyzed Composition (wt.%)		
	Li	Ca	Zn
Zn0.8Li	0.79	N/A	Balance
Zn0.1Li0.1Ca	0.10	0.11	Balance
Zn0.1Li0.4Ca	0.10	0.42	Balance
Zn0.1Li0.8Ca	0.11	0.84	Balance
Zn0.4Li0.1Ca	0.38	0.10	Balance
Zn0.4Li0.4Ca	0.39	0.42	Balance
Zn0.8Li0.1Ca	0.81	0.09	Balance
Zn0.8Li0.4Ca	0.79	0.45	Balance
Zn0.8Li0.8Ca	0.81	0.80	Balance

2.2. Microstructural characterization

An optical microscope (BX51 M, Olympus) to acquire the alloys' metallographic structures. Specimens were firstly being polished through a series of sandpapers (400#, 1200#, 2000#, 5000# and 7000#) to get a smooth surface. Then they were successively etched in 4% nital, rinsed by ethanol, and dried in the air. The metallographic structures of both as-cast and as-extruded alloys were obtained. The alloys' phase compositions were analyzed by an X-ray diffractometer (XRD DMAX 240, Rigaku) equipped with Cu Kα radiation, with a scan rate of 4°/min.

2.3. Mechanical tests

Specimens were prepared in accordance with ASTM-E8-04a for mechanical tests. A universal material testing machine (Instron 5969, USA) was used to implement the tensile tests, with a displacement rate of 1×10^{-4} s^{-1}. The mechanical properties obtained from the tests involve yield strength (YS), ultimate tensile strength (UTS), and the elongation (δ). A microhardness tester (SHIMADZUHMV-2t) was used to gauge the Vickers hardness, loading for 15s at a force of 0.1 kN.

2.4. In vitro degradation tests

2.4.1. Electrochemical tests

The electrochemical tests were carried out with a three-electrode cell system. The electrodes were as follows: a platinum electrode was chosen as counter electrode (CE), a saturated calomel electrode (SCE) was chosen as reference electrode (RE), and specimens being tested were designated as working electrodes (WE). The filling solution of the cell system is simulated body fluid (SBF) solution, whose composition [63,64] is: NaCl 8.035 g L^{-1}, $NaHCO_3$ 0.355 g L^{-1}, KCl 0.25 g L^{-1}, $K_2HPO_4{\cdot}3H_2O$ 0.231 g L^{-1}, $MgCl_2{\cdot}6H_2O$ 0.311 g L^{-1}, HCl (36–38%) 39 ml L^{-1}, $CaCl_2$ 0.292 g L^{-1}, Na_2SO_4 0.072 g L^{-1}, Tris 6.118 g L^{-1}. The pH of the solution is adjusted to 7.4. The electrochemical tests were conducted on an electrochemical workstation (Autolab, Metrohm, Switzerland) at room temperature.

2.4.2. In vitro degradation tests

The *in vitro* degradation tests were implemented by immersing the specimens into the SBF solution at 37 °C for 90 days (≈12 weeks). In the light of ASTM-G31-72, the solution to area ratio was set at 20 ml cm^{-2}. The solution was refreshed when precipitates appeared in the solution, lest they might disturb the degradation process. The discarded solution's pH value was measured at the meantime.

After 90 days of immersion, the specimens were rinsed with deionized water and dried in the air. Then the degradation products were analyzed. An SEM (S-4800, HITACHI, Japan) equipped with energy dispersive spectrometer (EDS) was used to obtain the microscopic images and the chemical composition. An X-ray diffractometer (XRD DMAX 240, Rigaku) was used to detect the crystal structure. Fourier transform infrared spectrometer (FTIR) method was employed to analyze the characteristic chemical groups.

After these analyses, the degradation products were cleaned with chromic acid (200 g/L CrO_3). Both before and after the cleaning, the morphology of the specimens were imaged. The macro-scale images were taken using a 2.5 dimensional high precision imaging instrument, and the micro-scale images were taken under the SEM. Before the degradation and after the cleaning, the specimens' weights were measured. And the degradation rates could be calculated using this equation: $C = \Delta m/(\rho \times A \times T)$, where C is the degradation rate (mm/year), Δm is the weight loss (g), ρ is the density of materials, A is the surface area of specimens, and T is the time of *in vitro* degradation tests.

2.5. In vitro biocompatibility tests

2.5.1. Cell viability tests

Before the tests, the cell culture was prepared by adding the alpha-minimum essential medium (α-MEM) with 10% fetal bovine serum (FBS) and 1% penicillin-streptomycin. The cytotoxicity tests and to evaluate the morphology of cytoskeleton were evaluated using osteoblast precursor cell line (MC3T3-E1, ATCC CRL-2594™). The alloy specimens were immersed in the cell culture medium to prepare the extracts of alloys at 37 °C for 24 h, with a volume to area ratio of 1.25 ml cm^{-2}. The extracting procedure was conducted in a humidified atmosphere with 5% CO_2. Then the supernatant was centrifuged and kept at 4 °C before usages.

MC3T3-E1 cells were seeded in 96-well plates, with a cell density of 3×10^4 per well. After 24 hours, the culture medium in each well was replaced with 100 μl of extracts, with a concentration at 100%, 50% and 10%, respectively. The negative control was selected as culture medium, and positive control group was selected as culture medium added with 10% dimethyl sulfoxide (DMSO, Invitrogen, USA). After 1, 2, and 4 days of incubation, the extracts were replaced with new culture medium added with 10 μl of Cell Counting Kit-8 (CCK-8, Dojindo Molecular Technologies, Japan) per well. After incubated for 1 h, a microplate reader (Bio-RAD680) was employed to gauge the optical density value (OD value) at the wavelength of 450 nm. For each group, at least 5 parallel measurements were taken.

2.5.2. Hemocompatibility tests

The hemocompatibility tests are conducted according to ISO 10993-4. Fresh blood of healthy New Zealand rabbits was collected, added with 3.8% (wt.%) sodium citrate at a volume ratio of 9:1.

For hemolysis tests, fresh blood was diluted by physiological saline solution at a ratio of 4:5. For each group, three parallel samples were used. Physiological saline was used as negative control, and deionized water was used as positive control. Samples of each group were first immersed in 15 ml saline at 37 °C for 30 min. Then in each centrifuge tube 0.2 ml of diluted blood was added in. After incubated at 37 °C for 60 min, with samples being removed, the tubes were centrifuged at 3000 rpm for 5 min. Then the supernatant was carefully transferred into 96-well plates and spectrophotometrical absorbance of each well was measured by a microplate reader (Bio-RAD680) at the wavelength of 545 nm. The hemolysis was calculated from this equation:

$$Hemolysis\ \ rate = \frac{OD(testing\ \ group) - OD(negative\ \ group)}{OD(positive\ \ group) - OD(negative\ \ group)} \times 100\%$$

For platelet adhesion test, the fresh blood was first centrifuged at 1000 rpm for 15 min, and platelet-rich plasma (PRP) was obtained from the supernatant. Samples were placed into 24-well plates, and in each well 0.4 ml PRP was added to allow a sufficient contact with the sample. After incubated at 37 °C for 60 min, the samples were gently rinsed with PBS. Subsequently they were fixed with 2.5% glutaraldehyde solution for 60 min, dehydrated with gradient ethanol solutions (50%, 60%, 70%, 80%, 90%, 95%, 100%) for 10 min each, and dried in the air. The morphologies of platelets on samples were observed using an SEM.

2.5.3. Cell morphology evaluation

DAPI and FITC (Sigma-Aldrich, Germany) were used to conduct the cytoskeletal staining. Based on the results of CCK-8 tests, alloy extracts of 50% concentration were chosen to culture the MC3T3-E1 cells for 24 h. A confocal laser scanning microscope (A1R–Si, Nikon, Japan) was used to observe the stained cells.

2.6. In vitro osteogenic differentiation tests

2.6.1. Osteogenesis-related gene expression studies

Real-time PCR method was applied to illustrate the expression mechanism of osteogenesis-related genes in MC3T3-E1 cells. Cells were seeded and cultured in the same way as ALP tests. Based on the ALP activity results, extracts were diluted to 50% and 25% as to prepare the osteogenic induction solution. The entire induction process lasted for 10 days, with culture medium refreshed every 48 hours. Subsequently, the mRNA expression levels of four marker *genes*: alkaline phosphatase (ALP), collagen type 1 (COL-1), osteocalcin (OCN) and Runt-related transcription factor 2 (Runx-2), were measured. Firstly, total RNA was extracted using RNeasy Mini Kit (Qiagen). Secondly, 1 mg RNA was reversed using a Reverse Transcription Kit (SuperScript™ III Reverse Transcriptase). The primer sequences are as shown in Supplementary Table 1. Thirdly, using the SYBR Premix Ex Taq II (2 ×) as PCR reagent, the real-time PCR was conducted on a ABI 7500 Fast machine (Applied Biosystems, Countaboeuf, France), under the conditions as-followed: 95 °C 30s; 95 °C 5s + 60 °C 40s, 40 cycles; dissolution curve, 95 °C 15s + 60 °C 60s + 95 °C 15s. Finally, the results were calculated through the $2^{-\Delta\Delta CT}$ method [39].

2.7. In vivo bone regeneration studies

2.7.1. Implants preparation

According to the former results of *in vitro* studies, Zn0.8Li0.1Ca alloy was selected to conduct further *in vivo* investigations. Pure Ti, the gold standard material in orthopedics, was chosen as the control group. Firstly, both as-extruded Zn0.8Li0.1Ca alloy and commercial pure Ti specimens were manufactured into cylinder (Φ = 3 mm, Height = 10 mm). Then, laser cauterization (TruLaser Tube 5000 fiber, Germany) was employed to drill through-holes (Φ = 0.5 mm) on the specimens to create porous scaffolds. There are six rows of through-holes on the side face and one through-hole on the center of bottom faces. The interval between holes on the side face is 0.5 mm. The porosity is calculated to be 23.27%. The size and appearance of the porous scaffold are as shown in Fig. S1.

2.7.2. Procedures of animal model establishment

In order to evaluate the bone-defect-treating effects of Zn0.8Li0.1Ca alloy, a rabbit radial bone defect model was employed. A total of 20 male New Zealand rabbits, each weighting about 2.5 kg, were recruited for the experiments. Firstly, the rabbits were anesthetized by injecting ketamine (10 mg/kg, Shanghai Ziyuan Pharmaceutical Co., Ltd, Shanghai, China) and 2% xylazine (5 mg/kg, Bayer, Leverkusen, North Rhine-Westphalia, Germany) through ear vein. Each rabbit's right anterior limb was fixed (at a flexed position), shaved and depilated. Then, an incision about 2 cm long was introduced parallel to the radial bone. The muscles were bluntly separated along the intermuscular spatium, exposing the diaphysis of radial bone. Using a pendulum saw, the diaphysis of radial bone was broken, and a bone defect about 10 mm long was created at the middle part of the diaphysis. Then the porous scaffolds were implanted inside. An illustration of the surgery procedure was shown in Fig. S2. An X-ray scan was given to each rabbit to examine the situation of surgery. Subsequently, each rabbit was injected with a 0.3 mg/kg dose of buprenorphine (Temgesic, Reckitt &Cloman, Hull, UK) as postoperative analgesia. The rabbits were then carefully fed. Among the rabbits, 10 were implanted with Zn0.8Li0.1Ca alloy scaffolds, and 10 were implanted with pure Ti scaffolds as control group. The rabbits would be sacrificed after 12 or 24 weeks of the surgery, respectively. Therefore, in each group at each time point there were 5 rabbits set as parallel groups. All these operations and experiments had been ratified by the Animal Ethics Committee of Jambo Biological Technology Co. Ltd, Shanghai, China.

2.7.3. X-ray observation and micro-computed tomography (Micro-CT)

At each time point (12 weeks or 24 weeks after the surgery), 5 rabbits of each group were selected to evaluate the conditions of bone remodeling. Firstly, an X-ray scan was given to each animal. Then the rabbits were sacrificed. The radius and ulnar bones of their right anterior limb were explanted and fixed in 4% paraformaldehyde. The radial bones

then underwent an examine through Micro-CT (Scanco Micro-CT100, Switzerland). After that, 3D reconstruction (Scanco μ100 evaluation software) was performed to evaluate the conditions of the bone remodeling and the biodegradation of the scaffolds. Region of interests (ROI) were defined as the circular bone tissue around the scaffolds within 0.5 mm. Indices about osteogenesis, including BMD (Bone Mineral Density), BV/TV (Percentage of Bone volume to Total volume), Tb.N (Trabecular Number), Tb.Th (Trabecular Thickness), and Tb.Sp (Trabecular Separation) were quantitatively analyzed for the ROIs.

2.7.4. Histological evaluation

After the Micro-CT scan, hard tissue slices were prepared. The specimens were firstly fixed with paraformaldehyde. Then, the specimens were rinsed with water, dehydrated with ethanol, cleaned with xylene, and finally embedded with methyl methacrylate (MMA). The cutting direction was perpendicular to the bone's long axis. Then slices were performed with Paragon staining, Van Gieson staining, and toluidine blue staining, respectively. After that, a high-resolution microscope (Olympus Co., Ltd., Tokyo, Japan) was applied to acquire the images of slices. Then, an SEM equipped with EDS was used to analyze the distributions of elements.

2.7.5. In vivo biocompatibility evaluation

After the surgery, crucial indicators of animals, including body

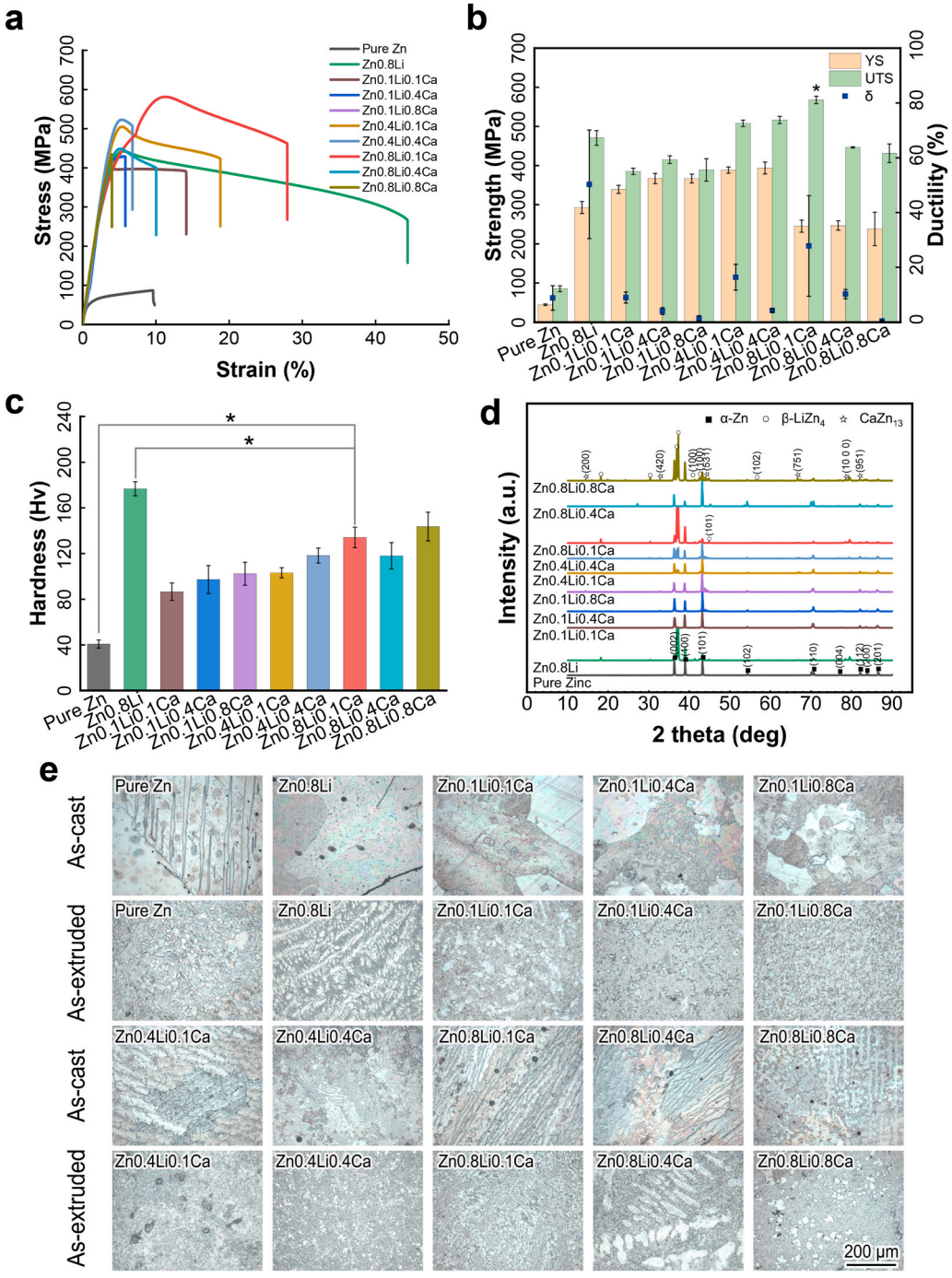

Fig. 1. Mechanical properties and microstructures. (a) Stress-strain curves; (b) Mechanical strength and elongation; (c) Vickers hardness; (d) X-ray diffraction; (e) Metallographic analyses. The data were expressed as mean ± standard deviation (SD). n = 4 in panel (b); n = 10 in panel (c). *: $p < 0.05$.

temperature, body weight and wound healing conditions were recorded everyday. Twenty-four weeks after the implantation, biological samples were collected from both the Zn0.8Li0.1Ca alloy group and the pure Ti group, to evaluate the materials' *in vivo* biocompatibility. Firstly, cardiac blood as well as visceral organs, including the heart, liver, spleen, lung and kidney were collected from the rabbits. An ICP-Mass Spectrometry (ICP-MS, NexION 300Â, USA) was used to gauge the concentrations of Zn^{2+}, Li^{+} and Ca^{2+} in the blood serum. The organ tissues were prepared into slices and performed with H&E staining. The pathological conditions were evaluated using an optical microscope. Blood biochemistry tests were carried out for each group. The 15 indices being analyzed comprise alanine aminotransferase (ALT), transglutaminase (AST), direct bilirubin (DBIL), total bilirubin (TBIL), albumin (ALB), alkaline phosphatase (ALP), gamma -glutamyl transpeptidase (Γ-GT), blood urea nitrogen (BUN), creatinine (CRE), uric acid (UA), total biliary acid (TBA), creatine kinase (CK), myocardial band of creatine kinase (CK-MB), L-lactate dehydrogenase (LDH-L) and lactate dehydrogenase-1 (LDH-1).

2.8. Statistical analysis

The data were analyzed via one-way analysis of variance (ANOVA) followed by Tukey post hoc tests. The results were presented as mean ± standard deviation ($n \geq 3$, independent samples). A *p-value < 0.05 was considered significant.

3. Results

3.1. Mechanical properties and microstructures

3.1.1. Mechanical properties

Fig. 1(a) and (b) show the mechanical properties of as-tested Zn alloys. The highest ultimate tensile strength belongs to Zn0.8Li0.1Ca alloy (567.60 ± 9.56 MPa), which is 20.64% higher than the UTS of Zn0.8Li alloy (470.49 ± 18.8 MPa). Zn0.8Li0.1Ca has a lower YS (245.22 ± 15.40 MPa) than that of Zn0.8Li (292.80 ± 15.31 MPa). For metallic materials without a clear yield platform, the yield strength (YS) is usually determined as where the 0.2% plastic deformation occurred. As Fig. 1(a) shows, the slope of the stress-stress curve's elastic part (which represents for Young's modulus) of Zn0.8Li0.1Ca is lower than that of Zn0.8Li, which means Zn0.8Li0.1Ca has a lower Young's modulus. Also, the 0.2% plastic deformation would happen earlier for Zn0.8Li0.1Ca than Zn0.8Li. Besides, Zn0.8Li0.1Ca alloy owns the highest elongation (27.82 ± 18.35%) among the tertiary ZnLiCa alloys. The results of tensile tests manifest that Zn0.8Li0.1Ca alloy exhibits the best mechanical properties in the ZnLiCa alloy system. Fig. 1(c) shows the micro-hardness properties of the alloys. The hardness of Zn0.8Li0.1Ca alloy (134.10 ± 8.99 Hv) is significantly lower than that of Zn0.8Li binary alloy (176.70 ± 6.20 Hv).

3.1.2. Microstructures

Fig. 1(d) shows the XRD results of experimental ZnLiCa alloys. The main phases are α-Zn, β-$LiZn_4$, and $CaZn_{13}$. Fig. 1(e) shows the microstructures of Zn alloys acquired from metallographic analyses. Both the as-cast and as-extruded ZnLiCa alloys were analyzed. The as-cast alloys exhibit larger grains. With the alloying elements increasing, there appeared dendritic structures in the alloys. After the extrusion process, the grains were refined. In the alloys with higher Ca element content (0.4%, 0.8%), there appeared more second phases in the shape of square or with straight edges. In the alloys with higher Li element content (0.4%, 0.8%), there are more phases of lamellar structures. Zn0.8Li0.1Ca alloy exhibits a river-like pattern, which consists of dense lamellar grains, similar to that of Zn0.8Li. Previous study have proved that the Zn0.8Li exhibits a typical hypereutectic microstructure of β-$LiZn_4$ and Zn [21]. And the addition of Ca element have brought an obvious grain refinement to the Zn0.8Li0.1Ca alloy, without generating large grains of second phases. Having a uniform and refined micro-structure suggests that Zn0.8Li0.1Ca alloy might possess better mechanical properties.

3.2. In vitro degradation behavior analyses

3.2.1. Electrochemical tests

Fig. 2(a) and Fig. S2(a) show the Tafel polarization curves obtained from the electrochemical tests. The open circuit potential (OCP) of Zn0.8Li0.1Ca alloy is lower than those of pure Zn and Zn0.8Li alloy. Fig.2(b) and Fig. S2(b) show the Nyquist curves obtained from the impedance spectroscopy tests, in which the impedance spectroscopy loop of Zn0.8Li0.1Ca alloy is smaller than those of pure Zn and Zn0.8Li alloy. The results of electrochemical tests show that the resistance to degradation of Zn0.8Li0.1Ca alloy is much smaller than pure Zn and Zn0.8Li alloy.

3.2.2. In vitro degradation tests

Fig. 2(c) shows the *in vitro* degradation rates calculated through the mass loss method. Zn0.8Li0.1Ca alloy exhibits a higher degradation rate (17.77 ± 2.75 μm $year^{-1}$) than that of pure Zn (12.97 ± 1.68 μm $year^{-1}$). This is consistent with the results of electrochemical tests. Fig. 2(d)(e) and Fig.S3(a)(b) show the degradation morphology after 90 days of immersion tests. It can be seen that there are more degradation products on the surface of Zn0.8Li0.1Ca alloy than pure Zn and Zn0.8Li alloy. After being cleaned, it can be seen that the surface of Zn0.8Li0.1Ca alloy is more coarse than the control groups.

3.2.3. Chemical analyses of the in vitro degradation products

Fig. 2(f) and (g) show the XRD and FTIR results of specimens after the degradation tests. Comparing Figs. 1(d) and Fig.2(f), it can be seen that there appeared two new phases, ZnO and $CaCO_3$, after the degradation test. Fig. 2(g) shows that the main chemical groups of degradation products are H–O, CO_3^{2-}, PO_4^{3-}, and Zn–O. From these results of chemical analyses, it can be determined that ZnO and $CaCO_3$ are the degradation products of ZnLiCa alloys in SBF.

3.3. In vitro biocompatibility

3.3.1. Cell viability tests

Fig. 3(a)(b) and Fig. S4 show the results of CCK-8 tests. The viability of MC3T3-E1 cells were inhibited when cultured in 100% extracts. For the extracts of 50% and 10% concentration, there exhibited no significant difference in the cells' viabilities between the ZnLiCa alloy groups and the negative control group (cultured in α-MEM).

3.3.2. Hemocompatibility tests

Fig. 3(c) shows the results of hemolysis tests. The hemolysis rates of all Zn alloys are below 5%. There exhibits no significant difference between the results of Zn alloys and the negative group (physiological saline), which are significantly lower than the positive group (deionized water). Fig. 3(d) shows the morphology of platelet adhesion on the surface of Zn alloys. There are no obvious activation of platelets on these Zn alloys. These results show that ZnLiCa alloys exhibit good hemocompatibility.

3.3.3. Cell morphology evaluation

Fig. 4(a) show the cell morphology obtained from cytoskeletal staining. The MC3T3-E1 cells of pure Zn and Zn0.8Li alloy groups exhibit a lower cell number, and the cells were not well spread. Compared to these two control groups, the cells in Zn0.8Li0.1Ca alloy group showed a heathier spreading state. Also the cells are denser in the Zn0.8Li0.1Ca group.

3.3.4. Osteogenesis-related gene expression

Fig. 4(b)–(e) show the expression results of four osteogenesis-related

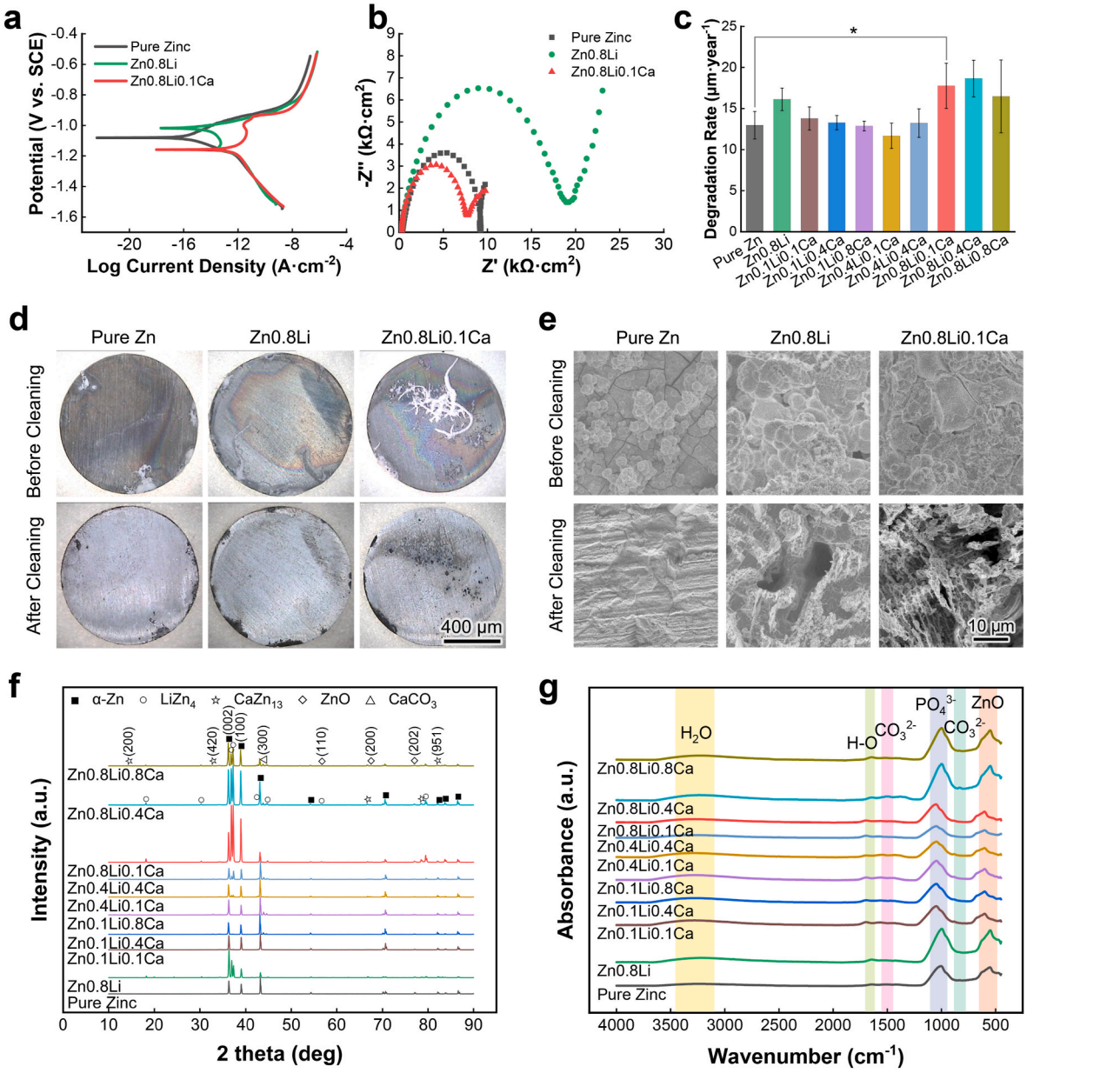

Fig. 2. Electrochemistry and *in vitro* degradation tests. (a) Tafel polarization curves; (b) Impedance spectroscopy; (c) Degradation rates calculated through weight loss method; (d) Degradation morphology in macro-scale; (e) Degradation morphology under SEM; (f) XRD results of degradation products; (g) FTIR results of degradation products. The data (n = 5) were expressed as mean ± standard deviation (SD). *: $p < 0.05$.

genes, namely ALP, COL-1, OCN, and Runx-2. For all these four genes, the Zn0.8Li0.1Ca alloy group exhibits the highest expression level compared to other three control groups. Especially, the expression level of OCN in the Zn0.8Li0.1Ca alloy group is significantly higher than other groups. For 50% extracts, the OCN expression level of Zn0.8Li0.1Ca alloy group (2.37 ± 0.05) is almost twice that of the Zn0.8Li alloy group (1.19 ± 0.07). For 25% extracts, the OCN expression level of Zn0.8Li0.1Ca alloy group (8.25 ± 0.83) is almost triple that of the Zn0.8Li alloy group (2.85 ± 0.09).

3.4. X-ray imaging and micro-CT

3.4.1. The repair conditions of bone defects

Fig. 5(a) shows the X-ray results of the limb implanted with porous scaffolds right after the surgery, 12 weeks later, and 24 weeks later, respectively. Fig. 5(c) shows the results of micro-CT 3D reconstruction at the same time of 12 weeks and 24 weeks post-surgery. At 12 weeks, there still exist gaps between the pure Ti scaffold and the bone, showing that the scaffold was not well integrated with the surrounding bone tissue. At the same time, the Zn0.8Li0.1Ca alloy scaffold has already been surrounded by new bone tissue. From the reconstructions of ROIs and new bone tissue (the 3rd and 4th row of panels in Fig. 5(c)), it can be seen that new bone tissue has grown into the pores of Zn0.8Li0.1Ca alloy scaffold, which was not observed in the pure Ti group. At 24 weeks, the bone tissue surrounding the Zn0.8Li0.1Ca alloy scaffold became more massive. While the pure Ti scaffold has not been completely integrated with the bone. These results show that the bone defect repair is more rapid in the Zn0.8Li0.1Ca alloy group than in the pure Ti group, and the integration conditions were also better in the Zn0.8Li0.1Ca alloy group.

3.4.2. Analyses of osteogenesis indices acquired from Micro-CT

Fig. 5(b) shows the quantitative analyses of osteogenesis-related indices acquired through micro-CT. For BV, BV/TV and Tb.N, both at 12 weeks and 24 weeks, the data of Zn0.8Li0.1Ca alloy groups are

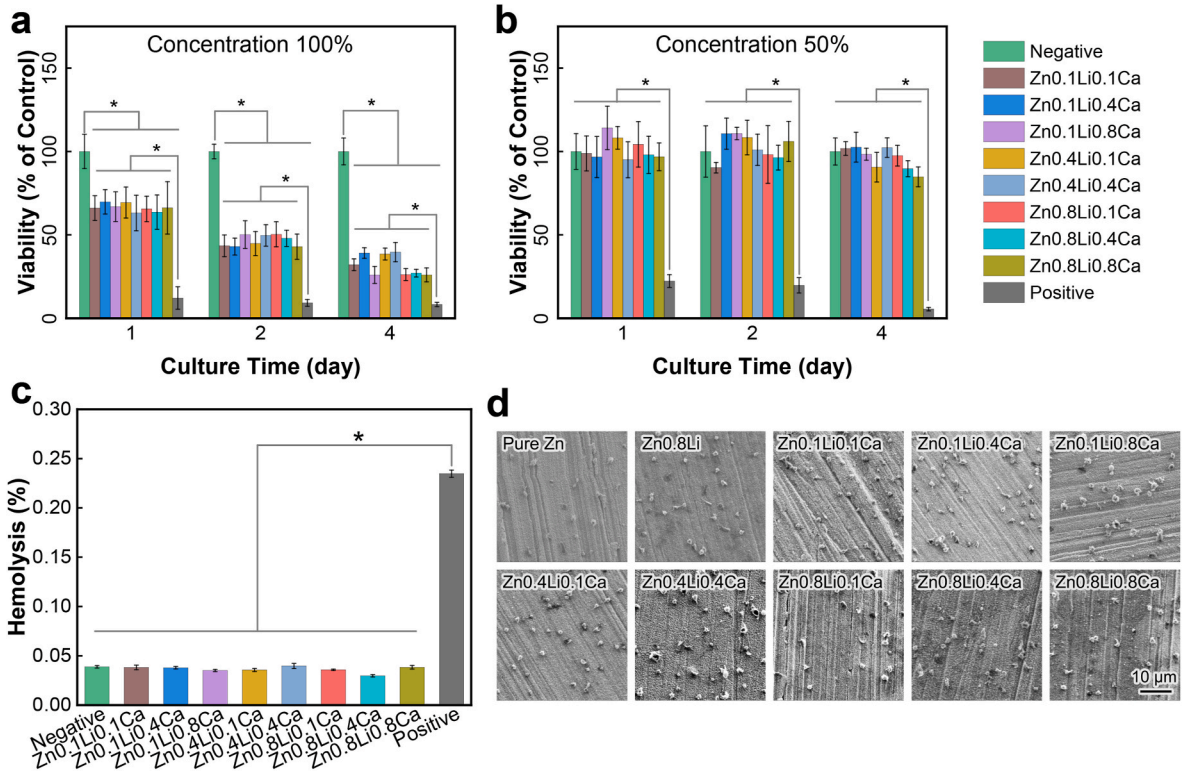

Fig. 3. *In vitro* biocompatibility test. (a) CCK-8 results of 100% extracts; (b) CCK-8 results of 50% extracts; (c) Hemolysis rates; (d) Morphology of platelet adhesion. The data were expressed as mean ± standard deviation (SD). n = 5 in panels (a) (b); n = 3 in panels (c). *: $p < 0.05$.

significantly higher than those of pure Ti groups. The Tb.Th of Zn0.8Li0.1Ca alloy group is significantly higher than that of pure Ti group at 12 weeks. The Tb.Sp of Zn0.8Li0.1Ca alloy group is lower than that of pure Ti group, in another word, the density of trabecula is higher in the Zn0.8Li0.1Ca alloy group. These quantitative analyses reveal that the regeneration of bone defects is better in the Zn0.8Li0.1Ca alloy group than the pure Ti group.

3.4.3. *In vivo biodegradation of the porous scaffolds*

The 5th row of panels in Fig. 5(c) shows the reconstructions of implanted porous scaffolds. Obviously, the pure Ti scaffold remained intact after 12 and 24 weeks of the surgery. For the Zn0.8Li0.1Ca alloy group, the positions of the scaffolds' pores were recognized as metallic materials, which means the scaffolds were biodegraded and there were biodegradation products in the pores. Besides, the surface of the Zn0.8Li0.1Ca alloy scaffold is also rougher than that of the pure Ti scaffold. These results illustrate that there occurred biodegradation for the Zn0.8Li0.1Ca alloy group while the pure Ti scaffold showed no such evidence.

3.5. *Histological evaluation*

3.5.1. *Histological evaluation of tissue hard-tissue slices*

Fig. 6(a) shows the Paragon staining results of hard-tissue slices. During the regeneration of bone defect, new bone tissue would grow into the pores of the scaffolds. And the Paragon staining method could stain the osteoblasts into violet. At 12 weeks, the staining of new bone tissue in the Zn0.8Li0.1Ca alloy scaffold was obviously darker than that of the pure Ti group, which means there were more osteoblasts in the Zn0.8Li0.1Ca alloy group. At 24 Weeks, both the staining of the two groups became darker. However, the staining in the Zn0.8Li0.1Ca alloy group was darker than that of the pure Ti group. Besides, there occurred biodegradation in the Zn0.8Li0.1Ca alloy scaffold, while there were no significant biodegradation products in the pure Ti scaffold.

Fig. 6(b) shows the Van Gieson staining results. At 12 weeks, collagen tissue (the nuclei would be stained into blue, and reticular collagen would be stained into brown) had grown into the porous scaffolds of both groups. At 24 weeks, a small amount of new bone (stained into red) had grown into the pores of pure Ti scaffold. In contrast, the amount of new bone grown into the Zn0.8Li0.1Ca alloy scaffold was obviously larger than the pure Ti group.

Fig. 6(c) shows the Toluidine blue staining results, in which the new bone tissue would be stained into blue. For the pure Ti groups, both at 12 weeks and 24 weeks, there were only a slight amount of bone tissue grown into the porous scaffold. In contrast, for the Zn0.8Li0.1Ca alloy groups, new bone tissue started to grow into the scaffold at 12 weeks, and massive new bone tissue almost filled the pores of Zn0.8Li0.1Ca alloy scaffold at 24 weeks.

These results illustrated that the integration and growth conditions of new bone tissue were significantly better in the Zn0.8Li0.1Ca alloy scaffold than in the pure Ti group.

3.5.2. *Elements distribution of hard-tissue slices*

Fig. 7(a)(d) show the EDS mapping results of hard-tissue slices at 12 weeks and 24 weeks, respectively. The distribution of elements Ti, C, O, P, Ca, and Zn are as displayed. For the pure Ti group, both at 12 weeks and 24 weeks, there is a clear boundary of the distribution of element Ti, which indicate that the scaffold remained intact. For the Zn0.8Li0.1Ca alloy group, at 24 weeks, the scaffold was under biodegradation and a segment of the scaffold was embedded in the bone tissue.

Furthermore, line scan were conducted for each slice. The line scan directions are as displayed in Fig. 7(a)(d). Fig. 7(b)(d) show the 12 weeks' line scan results of pure Ti group and Zn0.8Li0.1Ca alloy group, respectively. Fig. 7(c)(f) show the 24 weeks' line scan results of pure Ti group and Zn0.8Li0.1Ca alloy group, respectively. As the line scan results show, in the pure Ti groups, there is a clear boundary between the metallic scaffold and the bone tissue, which is evidenced by the distribution of element Ti. While in the Zn0.8Li0.1Ca alloy groups, there

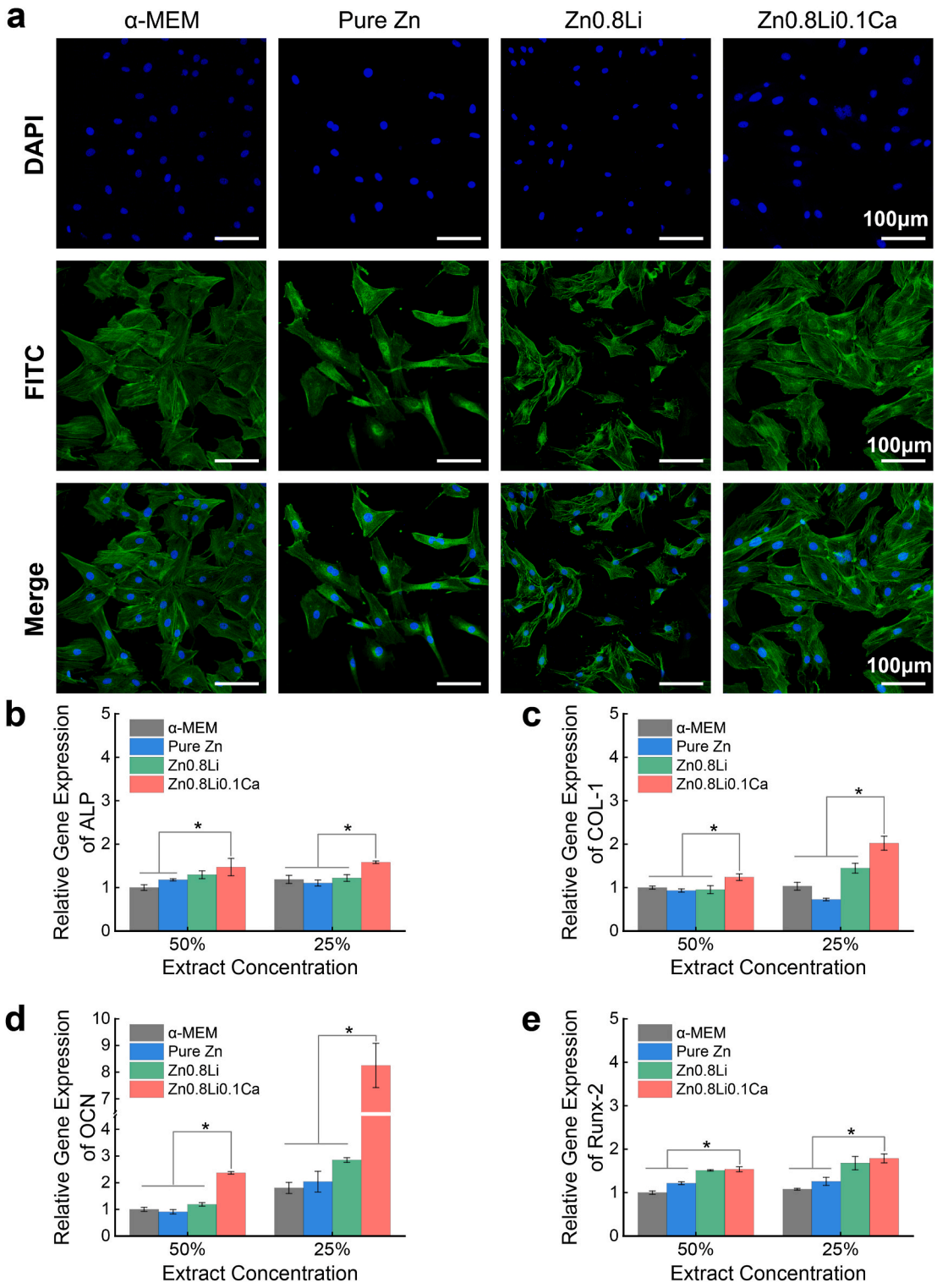

Fig. 4. Cell morphology and Osteogenesis-related genes expression. (a) Cytoskeletal staining; (b)–(e) The relative gene expression levels of ALP, COL-1, OCN and Runx-2. The data (n = 3) were expressed as mean ± standard deviation (SD). *: $p < 0.05$.

exists troughs for the signal intensity of element Zn, which indicates that the Zn0.8Li0.1Ca alloy underwent biodegradation and segments were separated from the scaffold.

3.6. *In vivo* biocompatibility

Fig. 8(a) shows the histological slices of collected organs from the sacrificed rabbits, including the heart, liver, spleen, lung and kidney. The H&E staining of organs show that there existed no obvious differences between the pure Ti group and Zn0.8Li0.1Ca alloy group. Fig. 8(b) shows the ICP results of Zn^{2+}, Li^{+}, and Ca^{2+} in the blood serum. The concentration levels of these three ions showed no significant differences. Fig. 8(c) shows the blood chemistry tests results. For all the fifteen items being tested, there were no significant differences between the two groups. All these results show that the pure Ti group and Zn0.8Li0.1Ca alloy group showed a similar level as to the *in vivo* biocompatibility.

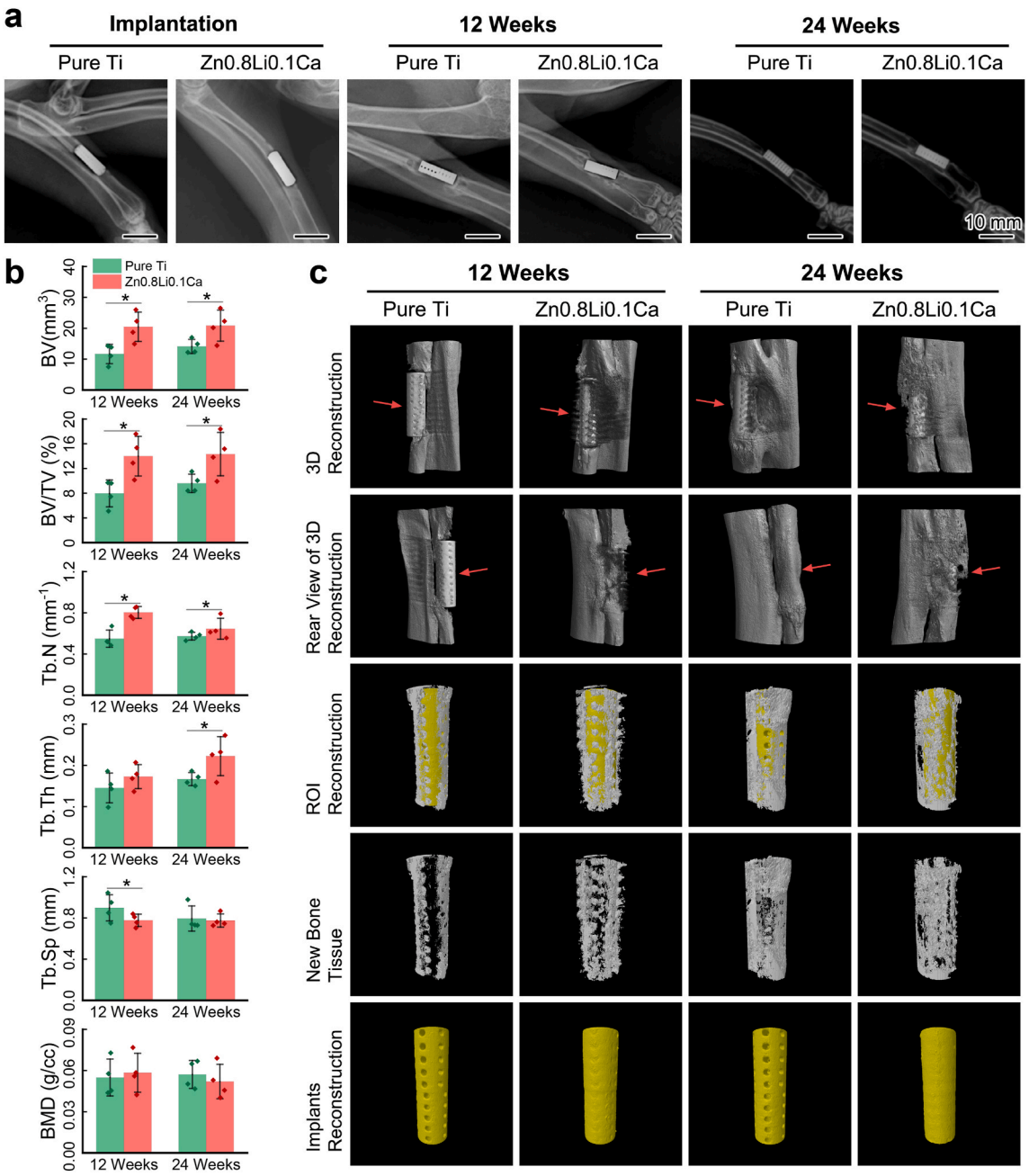

Fig. 5. Animal test results. (a) X-ray scanning images; (b) Quantitative analyses of osteogenesis indices calculated from Micro-CT; (c) Micro-CT 3D reconstructions. The data (n = 4) were expressed as mean ± standard deviation (SD). *: $p < 0.05$.

4. Discussion

The regeneration of bone defect is a complicated process, which involves intricate interactions between various cells, cytokines and signaling pathways [12]. The potential mechanism how Zn0.8Li0.1Ca alloy scaffold assisted the bone with regeneration might be explained in two aspects: providing structural supports and regulating physiological functions.

4.1. The structural supports of Zn0.8Li0.1Ca alloy scaffold

Biodegradable metals have been investigated, and were regarded as promising substitutes for traditional metallic materials in orthopedics since the last two decade. However, the applications of biodegradable metals are still very limited right now. One main reason is their unsatisfactory mechanical properties compared to the traditional metallic materials [45]. The mechanical strength of pure Ti, the gold standard material used in orthopedics, usually exceeds 500 MPa [65]. Nonetheless, the ultimate tensile strength of most previous biodegradable metals could not compete with this standard. For instance, the UTS of Mg-based biodegradable metals are below 350 MPa [13]. Among the previous studies, Zn–Li alloys possess the highest UTS. The UTS of Zn0.7Li could surpass 560 MPa [50]. However, the elongation of Zn0.7Li alloy is only 2%, far from meeting the clinical requirements.

In this paper, the ZnLiCa alloy system exhibits excellent mechanical properties. The UTS of Zn0.8Li0.1Ca alloy is 567.60 ± 9.56 MPa, which is comparable to that of pure Ti, and stronger than the aforementioned Zn0.7Li. The elongation of Zn0.8Li0.1Ca alloy is 27.82 ± 18.35%, which also meets the requirements of serving as biomaterials [66]. The mechanical properties of Zn0.8Li0.1Ca alloy render it a promising

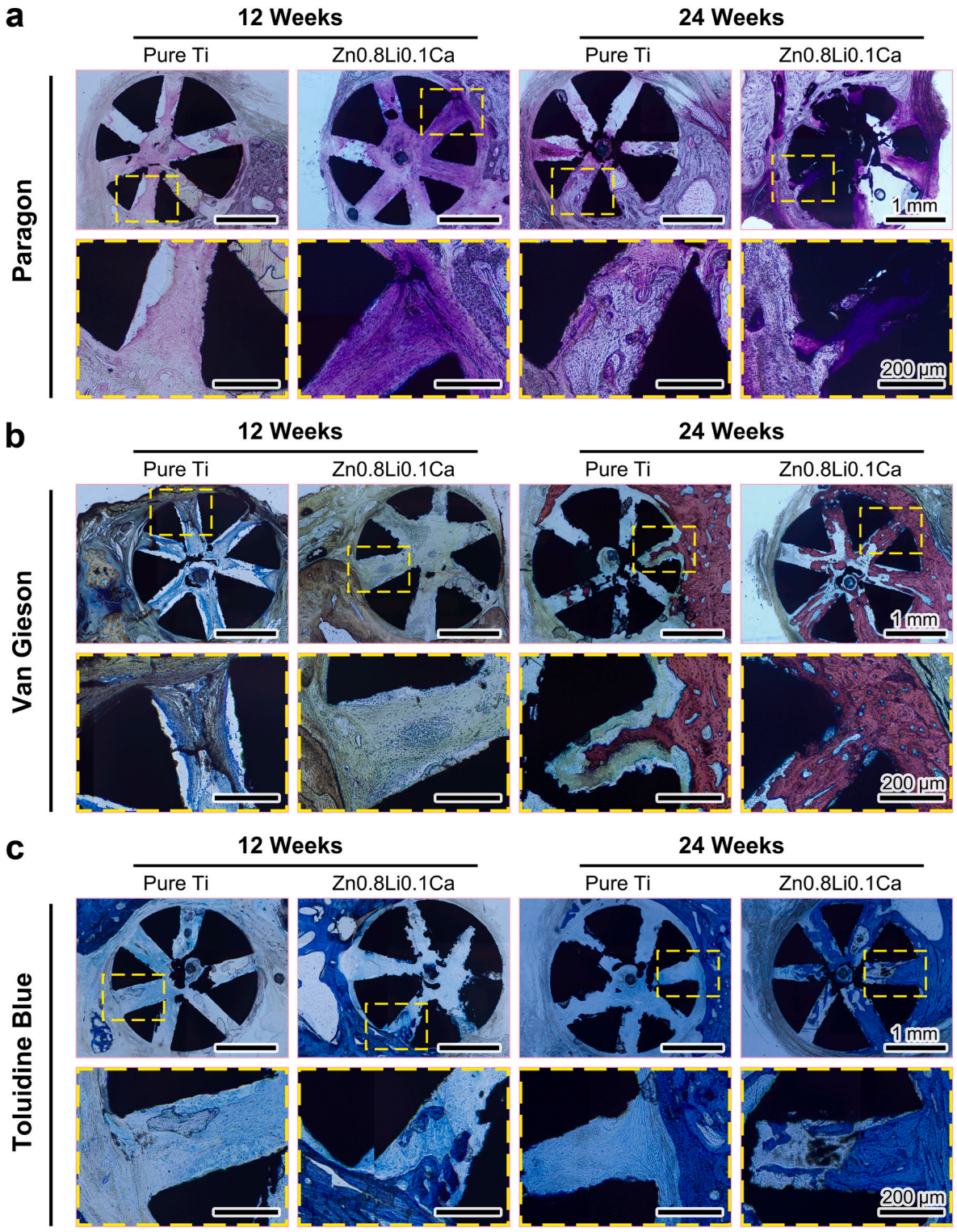

Fig. 6. Histological analyses of hard-tissue slices. (a) Paragon staining; (b) Van Gieson staining; (c) Toluidine blue staining.

candidate for clinical usages in orthopedics, especially at load-bearing positions.

A careful structural design of the scaffolds can provide favorable conditions for the bone to regain its vascularization. Firstly, the size of pore should be considered. Previous studies have shown that the blood vessel ingrowth would be significantly faster when the pore size was larger than 250 μm [67,68]. Besides, the interconnectivity of pores is also requisite for vascularization. A poor interconnectivity within the scaffold would retard the vascularization of blood vessel [69]. The Zn0.8Li0.1Ca alloy scaffold in this study was designed with rows of through-holes connected with each other, and the diameter of holes is 0.5 mm. This structural design would be beneficial for the regeneration of bone defect, which is verified by the *in vivo* results (Figs. 5 and 6).

Another problem should be considered in orthopedics is stress-shielding, which is usually caused by the over-high Young's modulus of the implants [70]. A porous structure design is helpful for reducing

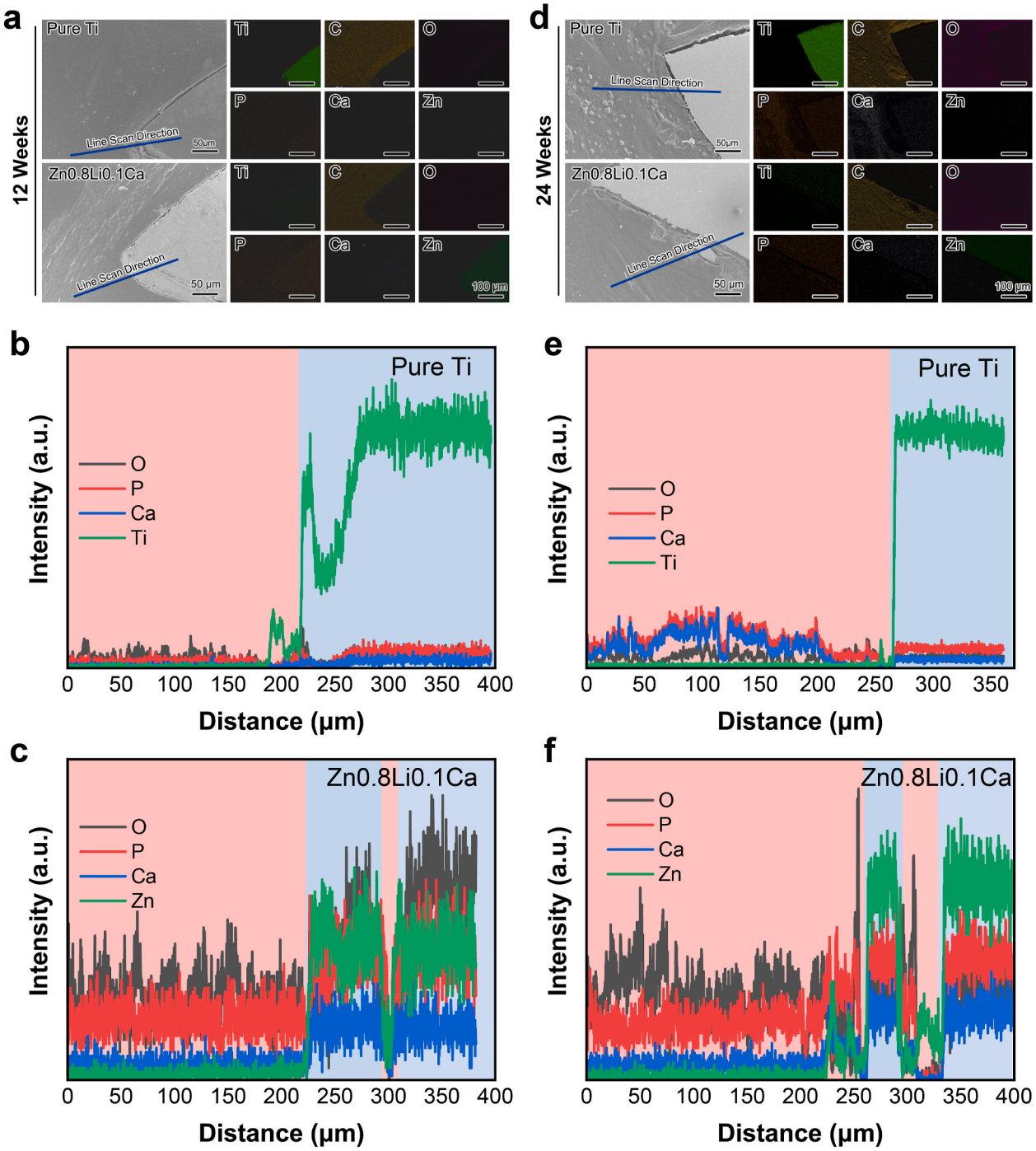

Fig. 7. Elements distribution analysis of hard-tissue slices. (a) EDS mapping of 12 weeks' results; (b) EDS line scan results of pure Ti group at 12 weeks; (b) EDS line scan results of Zn0.8Li0.1Ca alloy group at 12 weeks; (d) EDS mapping of 24 weeks' results; (e) EDS line scan results of pure Ti group at 24 weeks; (f) EDS line scan results of Zn0.8Li0.1Ca alloy group at 24 weeks.

the stiffness of the implants [71]. Besides, the biodegradation process would also decrease the mechanical strength gradually, leaving essential stress for the bone to restore to its own strength. These factors might also be beneficial to the regeneration of bone defects.

4.2. *The physiological functions of Zn0.8Li0.1Ca alloy scaffold*

The regeneration of bone defect is a very complex process, which could be generally divided into three consecutive stages, including the inflammatory stage, the callus stage, and the remodeling stage [72]. In the inflammatory stage, the damaged blood vessels will secrete platelet-derived growth factor (PDGF) and transforming growth factor-b1 (TGF-b1) [73,74]. At the same time, macrophages will gather and secrete transforming growth factor-β (TGF-β), insulin-like growth factors (IGFs), and fibroblast growth factor-2 (FGF2) [75]. These biological activities of these cytokines will trigger the formation of hematoma, recruit mesenchymal stem cells (MSCs), as well as start the cell proliferation and vascular ingrowth [76]. Subsequently, chondrocytes will produce cartilage which would form a fibrous callus [77]. The MSCs then proliferate and differentiate into osteoblasts, which would later transform the fibrous callus into woven bone callus [78]. Subsequently, the osteoclasts and osteoblasts will participate in the bone-remodeling

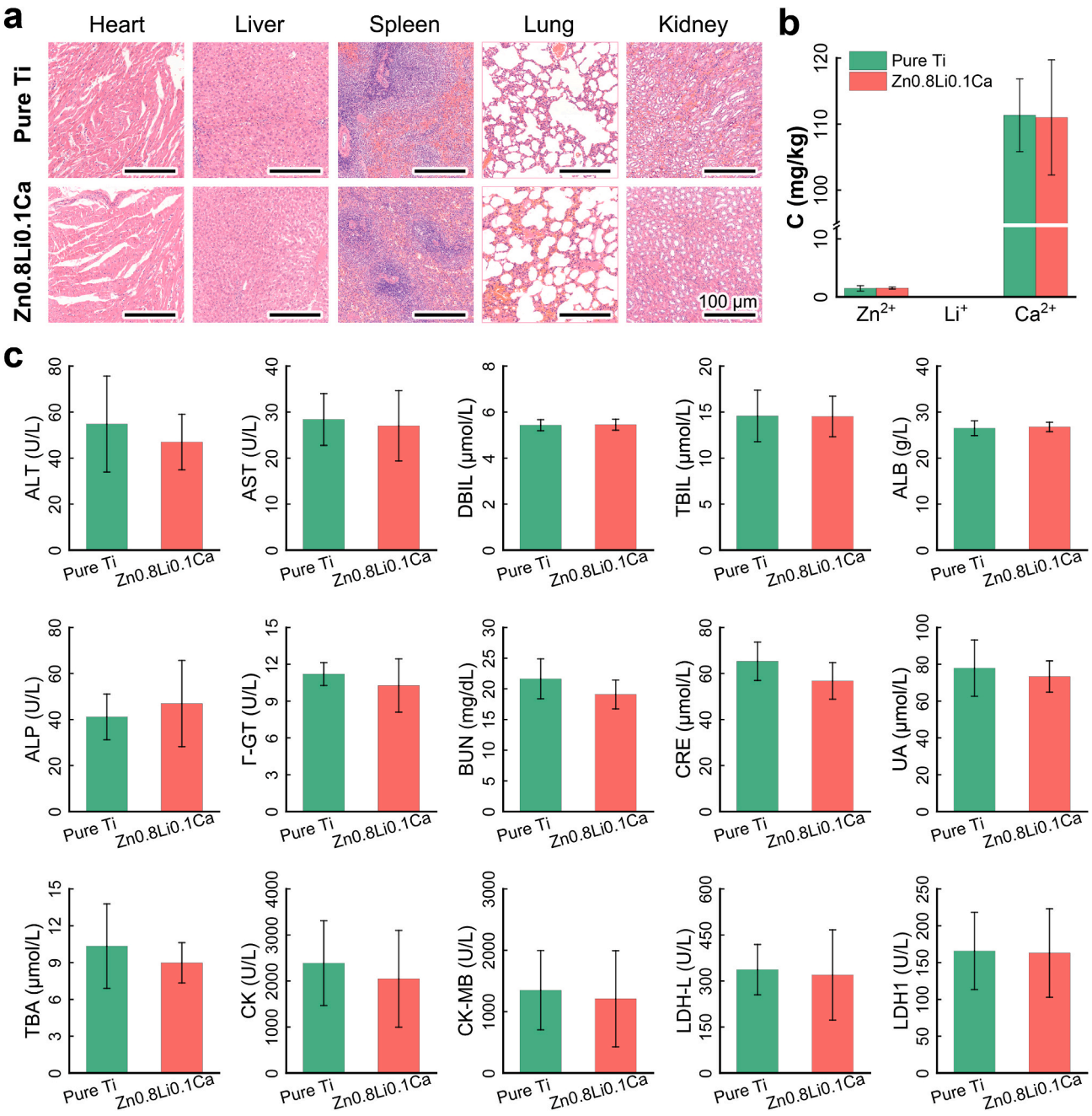

Fig. 8. *In vivo* biocompatibility. (a) Histological evaluations of organs; (b) ICP results of Zn^{2+}, Li^{+} and Sr^{2+} in blood serum (C: concentration); (c) Blood biochemistry test results. The data were expressed as mean ± standard deviation (SD). n = 3 in panel (b); n = 4 in panel (c). *: $p < 0.05$.

stage, during which the woven bone will finally transform into lamellar bone and restore to the initial healthy status [79].

After being implanted *in vivo*, the Zn0.8Li0.1Ca alloy scaffold would be biodegraded and release Zn^{2+}, Li^{+}, and Ca^{2+} to the extracellular environment, which would affect the cellular activities and the bone regeneration process.

Zn^{2+} can regulate the bone remodeling process through promoting the bone formation and attenuating the bone resorption simultaneously [80,81]. The expression levels of Runx-2 and Osterix, which are the master regulators in osteogenic process, can be improved by Zn^{2+} [82]. Runx-2 can improve the expression levels of ALP, COL-1 and OCN [83,84]. ALP and COL-1 are greatly expressed during the differentiation of osteoblasts, and OCN plays an important role in the mineralization of bone [85]. Through these pathways, Zn^{2+} can promote the bone formation. At a proper concentration, Zn^{2+} can accelerate the apoptosis of osteoclasts through NF-κB pathway, which would inhibit the bone resorption [86,87].

Li^{+} participate in the regulation of Wnt/β-catenin pathway [88,89], which plays an essential role in the proliferation of MSCs and the differentiation of osteoblasts [90]. Also, Li^{+} could inhibit the expression of adipogenic and osteoclastogenic factors [91], which would reduce the bone resorption. Also, Li^{+} can accelerate the callus ossification and bone healing in the later stage [92].

Calcium is the most common mineral in bone, and Ca^{2+} plays an important role in the regulation of the homeostasis of bone remodeling [93]. The extracellular Ca^{2+} can stimulate the calcium sensor receptor (CaSR), which is a critical receptor expressed both in mesenchymal lineage such as osteoblasts, and hematopoietic lineage such as osteoclasts [51,94]. Besides, Ca^{2+} can up-regulate the expression of osteocalcin (OCN) and contribute to the mineralization of bone [95]. The

optimum extracellular Ca^{2+} for the proliferation of osteoblasts is around 3–10 mM [94]. A higher Ca^{2+} concentration would inhibit the activity of osteoclast [96,97] and promote the proliferation and differentiation of osteoblasts [94,98]. During the bone resorption, osteoclasts can increase the extracellular Ca^{2+} concentration to 40 mM [99], which would trigger these activities. Similarly, the biodegradation of Zn0.8Li0.1Ca alloy can release Ca^{2+} into the extracellular environment and elevate the Ca^{2+} concentration, which would promote the activity of osteoblasts, reduce the activity of osteoclasts, and thus increasing the bone formation and inhibiting the bone resorption.

In this study, how the Zn0.8Li0.1Ca alloy helped bone defect regeneration was investigated both *in vitro* and *in vivo*. Firstly, real-time PCR was conducted to evaluate the expressions of four osteogenesis-related *genes*: ALP, COL-1, OCN and Runx-2. The results show that the expressions of all four *genes* were up-regulated in the Zn0.8Li0.1Ca group than the control groups. The expressions of COL-1 and OCN were especially high in Zn0.8Li0.1Ca group, suggesting that the biodegradation products of Zn0.8Li0.1Ca could promote the differentiation of osteoblasts and bone mineralization. Secondly, micro-CT was performed to evaluate the bone regeneration situations. The indices about osteogenesis in the Zn0.8Li0.1Ca group are higher than the pure Ti group. And the Zn0.8Li0.1Ca scaffold integrated better with the surrounding bone tissue. Thirdly, histological evaluations were conducted using the hard-tissue slices. All results show that the growth of new bone tissue was superior in the Zn0.8Li0.1Ca group than in the control groups. The results of this study are in line with the aforementioned studies.

The physiological functions of Zn^{2+}, Li^{+}, and Ca^{2+} are favorable for bone formation and inhibitory for the bone resorption, which would help the defect positions of bone to recover and maintain the regeneration. However, whether these ions would synergize and create a comprehensive effect still needs to be investigated. Besides, these functions of ions are temporary. When the Zn0.8Li0.1Ca alloy scaffold was totally biodegraded, the activities of osteoblasts and osteoclasts would return to their normal levels, which would not interrupt the bone hemostasis after the regeneration was accomplished.

5. Conclusion

In this paper, a novel biodegradable metal system, ZnLiCa, was developed and carefully researched, both *in vitro* and *in vivo*. Main conclusions can be drawn as followed:

(1) ZnLiCa biodegradable alloy system exhibit excellent mechanical properties. Among the experimental alloys, Zn0.8Li0.1Ca alloy exhibits the highest ultimate tensile strength (567.60 ± 9.56 MPa), which is 20.64% higher than that of Zn0.8Li alloy (470.49 ± 18.8 MPa).
(2) Zn0.8Li0.1Ca alloy accelerated the degradation rate compared with pure Zn and Zn0.8Li alloy, with an *in vitro* degradation rate of 17.77 ± 2.75 μm $year^{-1}$.
(3) Zn0.8Li0.1Ca alloy exhibits good biocompatibility both *in vitro* and *in vivo*. Zn0.8Li0.1Ca alloy could improve the expression level of osteogenesis-related genes (ALP, COL-1, OCN, Runx-2), especially the expression of OCN. The animal experiments show that Zn0.8Li0.1Ca alloy presented a similar biocompatibility level to pure Ti, while promoted the regeneration significantly faster than the pure Ti.

CRediT authorship contribution statement

Zechuan Zhang: Conceptualization, Methodology, Investigation, Writing – original draft, Data curation. **Bo Jia:** Conceptualization, Methodology, Investigation, Writing – review & editing. **Hongtao Yang:** Conceptualization, Methodology, Investigation. **Yu Han:** Investigation. **Qiang Wu:** Investigation. **Kerong Dai:** Conceptualization, Methodology, Resources, Supervision, Project administration, Funding acquisition. **Yufeng Zheng:** Conceptualization, Methodology, Resources, Supervision, Writing – review & editing, Project administration, Funding acquisition.

Declaration of competing interest

The authors declare that they have no known competing financial interests or personal relationships that could have appeared to influence the work reported in this paper.

This work was supported by National Natural Science Foundation of China (Grant No. 51931001), and International Cooperation and Exchange project between NSFC (China) and CNR (Italy) (NSFC-CNR Grant No. 52011530392).

Appendix A. Supplementary data

Supplementary data to this article can be found online at https://doi.org/10.1016/j.bioactmat.2021.03.045.

Acknowledgements.

References

[1] H. Zhou, J.G. Lawrence, S.B. Bhaduri, Fabrication aspects of PLA-CaP/PLGA-CaP composites for orthopedic applications: a review, Acta Biomater. 8 (6) (2012) 1999–2016.
[2] C.G. Trejo-Iriarte, J. Serrano-Bello, R. Gutierrez-Escalona, C. Mercado-Marques, N. Garcia-Honduvilla, J. Bujan-Varela, L.A. Medina, Evaluation of bone regeneration in a critical size cortical bone defect in rat mandible using microCT and histological analysis, Arch. Oral Biol. 101 (2019) 165–171.
[3] S. Kashte, R. Dhumal, P. Chaudhary, R.K. Sharma, V. Dighe, S. Kadam, Bone regeneration in critical-size calvarial defect using functional biocompatible osteoinductive herbal scaffolds and human umbilical cord Wharton's Jelly-derived mesenchymal stem cells, Materials Today Communications 26 (2021) 102049.
[4] W. Zhao, Z. Huang, L. Liu, W. Wang, J. Leng, Y. Liu, Porous bone tissue scaffold concept based on shape memory PLA/Fe3O4, Compos. Sci. Technol. (2020) 108563.
[5] G.J. Zeng, W.S. Foong, S. Xu, H.N. Pang, Induced membrane bone grafting technique for treatment of large postinfectious acetabular bone defects, Arthroplast Today 6 (3) (2020) 322–329.
[6] Z. Jamalpoor, H. Mirzadeh, M.T. Joghataei, D. Zeini, S. Bagheri-Khoulenjani, M. R. Nourani, Fabrication of cancellous biomimetic chitosan-based nanocomposite scaffolds applying a combinational method for bone tissue engineering, J. Biomed. Mater. Res. 103 (5) (2015) 1882–1892.
[7] M. Nabiyouni, T. Bruckner, H. Zhou, U. Gbureck, S.B. Bhaduri, Magnesium-based bioceramics in orthopedic applications, Acta Biomater. 66 (2018) 23–43.
[8] J. Zhou, X. Guo, Q. Zheng, Y. Wu, F. Cui, B. Wu, Improving osteogenesis of three-dimensional porous scaffold based on mineralized recombinant human-like collagen via mussel-inspired polydopamine and effective immobilization of BMP-2-derived peptide, Colloids Surf. B Biointerfaces 152 (2017) 124–132.
[9] Q. Chen, C. Zhu, G.A. Thouas, Progress and challenges in biomaterials used for bone tissue engineering: bioactive glasses and elastomeric composites, Prog Biomater 1 (1) (2012) 2.
[10] D. He, P. Liu, X. Liu, X. Chen, F. Ma, W. Li, C. Zhao, J. Tu, Hydroxyapatite bioceramic coatings prepared by hydrothermal-electrochemical deposition method, J. Wuhan Univ. Technol.-Materials Sci. Ed. 29 (2) (2014) 398–400.
[11] R.B. Minkowitz, S. Bhadsavle, M. Walsh, K.A. Egol, Removal of painful orthopaedic implants after fracture union, J. Bone Joint Surg. 89 (9) (2007) 1906–1912.
[12] B. Jia, H. Yang, Z. Zhang, X. Qu, X. Jia, Q. Wu, Y. Han, Y. Zheng, K. Dai, Biodegradable Zn–Sr alloy for bone regeneration in rat femoral condyle defect model: in vitro and in vivo studies, Bioactive Materials 6 (6) (2021) 1588–1604.
[13] Y.F. Zheng, X.N. Gu, F. Witte, Biodegradable metals, Mater. Sci. Eng. R 77 (2014) 1–34.
[14] Y. Liu, Y. Zheng, X.-H. Chen, J.-A. Yang, H. Pan, D. Chen, L. Wang, J. Zhang, D. Zhu, S. Wu, K.W.K. Yeung, R.-C. Zeng, Y. Han, S. Guan, Fundamental theory of biodegradable metals-definition, criteria, and design, Adv. Funct. Mater. (2019) 1805402.
[15] H.J. Seo, Y.E. Cho, T. Kim, H.I. Shin, I.S. Kwun, Zinc may increase bone formation through stimulating cell proliferation, alkaline phosphatase activity and collagen synthesis in osteoblastic MC3T3-E1 cells, Nutrition Research and Practice 4 (5) (2010) 356–361.
[16] K. Nakashima, X. Zhou, G. Kunkel, Z. Zhang, J.M. Deng, R.R. Behringer, B. De Crombrugghe, The novel zinc finger-containing transcription factor Osterix is required for osteoblast differentiation and bone formation, Cell 108 (1) (2002) 17–29.
[17] I.S. Kwun, Y.E. Cho, R.A. Lomeda, H.I. Shin, J.Y. Choi, Y.H. Kang, J.H. Beattie, Zinc deficiency suppresses matrix mineralization and retards osteogenesis transiently with catch-up possibly through Runx 2 modulation, Bone 46 (3) (2010) 732–741.
[18] H. Yang, C. Wang, C. Liu, H. Chen, Y. Wu, J. Han, Z. Jia, W. Lin, D. Zhang, W. Li, W. Yuan, H. Guo, H. Li, G. Yang, D. Kong, D. Zhu, K. Takashima, L. Ruan, J. Nie,

X. Li, Y. Zheng, Evolution of the degradation mechanism of pure zinc stent in the one-year study of rabbit abdominal aorta model, Biomaterials 145 (2017) 92–105.
[19] P.K. Bowen, R.J. Guillory 2nd, E.R. Shearier, J.M. Seitz, J. Drelich, M. Bocks, F. Zhao, J. Goldman, Metallic zinc exhibits optimal biocompatibility for bioabsorbable endovascular stents, Materials science & engineering, C, Materials for biological applications 56 (2015) 467–472.
[20] S. Zhao, J.M. Seitz, R. Eifler, H.J. Maier, R.J. Guillory 2nd, E.J. Earley, A. Drelich, J. Goldman, J.W. Drelich, Zn-Li alloy after extrusion and drawing: structural, mechanical characterization, and biodegradation in abdominal aorta of rat, Mater. Sci. Eng. C 76 (2017) 301–312.
[21] Z. Li, Z.Z. Shi, Y. Hao, H.F. Li, H.J. Zhang, X.F. Liu, L.N. Wang, Insight into role and mechanism of Li on the key aspects of biodegradable ZnLi alloys: microstructure evolution, mechanical properties, corrosion behavior and cytotoxicity, Materials science & engineering, C, Materials for biological applications 114 (2020) 111049.
[22] D. Vojtech, J. Kubasek, J. Serak, P. Novak, Mechanical and corrosion properties of newly developed biodegradable Zn-based alloys for bone fixation, Acta Biomater. 7 (2011) 3515–3522.
[23] E. Mostaed, M. Sikora-Jasinska, A. Mostaed, S. Loffredo, A.G. Demir, B. Previtali, D. Mantovani, R. Beanland, M. Vedani, Novel Zn-based alloys for biodegradable stent applications: design, development and in vitro degradation, Journal of the mechanical behavior of biomedical materials 60 (2016) 581–602.
[24] J. Kubasek, D. Vojtech, E. Jablonska, I. Pospisilova, J. Lipov, T. Ruml, Structure, mechanical characteristics and in vitro degradation, cytotoxicity, genotoxicity and mutagenicity of novel biodegradable Zn-Mg alloys, Mater. Sci. Eng. C 58 (2016) 24–35.
[25] H. Yang, X. Qu, W. Lin, D. Chen, D. Zhu, K. Dai, Y. Zheng, Enhanced osseointegration of Zn-Mg composites by tuning the release of Zn ions with sacrificial Mg-rich anode design, ACS Biomater. Sci. Eng. 5 (2) (2018) 453–467.
[26] X. Liu, J. Sun, F. Zhou, Y. Yang, R. Chang, K. Qiu, Z. Pu, L. Li, Y. Zheng, Micro-alloying with Mn in Zn–Mg alloy for future biodegradable metals application, Mater. Des. 94 (2016) 95–104.
[27] H.F. Li, X.H. Xie, Y.F. Zheng, Y. Cong, F.Y. Zhou, K.J. Qiu, X. Wang, S.H. Chen, L. Huang, L. Tian, L. Qin, Development of biodegradable Zn-1X binary alloys with nutrient alloying elements Mg, Ca and Sr, Sci. Rep. 5 (2015) 10719.
[28] N.S. Murni, M.S. Dambatta, S.K. Yeap, G.R. Froemming, H. Hermawan, Cytotoxicity evaluation of biodegradable Zn-3Mg alloy toward normal human osteoblast cells, Materials science & engineering, C, Materials for biological applications 49 (2015) 560–566.
[29] I. Pospíšilová, V. Soukupová, D. Vojtěch, Influence of calcium on the structure and mechanical properties of biodegradable zinc alloys, Mater. Sci. Forum 891 (2017) 400–403.
[30] Y. Zou, X. Chen, B. Chen, Effects of Ca concentration on degradation behavior of Zn-x Ca alloys in Hank's solution, Mater. Lett. 218 (2018) 193–196.
[31] G.-z. Ke, R. Yue, H. Huang, B. Kang, H. Zeng, G.-y. Yuan, Effects of Sr addition on microstructure, mechanical properties and in vitro degradation behavior of as-extruded Zn−Sr binary alloys, Trans. Nonferrous Metals Soc. China 30 (7) (2020) 1873–1883.
[32] J. Niu, Z. Tang, H. Huang, J. Pei, H. Zhang, G. Yuan, W. Ding, Research on a Zn-Cu alloy as a biodegradable material for potential vascular stents application, Mater. Sci. Eng. C 69 (2016) 407–413.
[33] Z. Tang, J. Niu, H. Huang, H. Zhang, J. Pei, J. Ou, G. Yuan, Potential biodegradable Zn-Cu binary alloys developed for cardiovascular implant applications, Journal of the mechanical behavior of biomedical materials 72 (2017) 182–191.
[34] X. Qu, H. Yang, B. Jia, Z. Yu, Y. Zheng, K. Dai, Biodegradable Zn-Cu alloys show antibacterial activity against MRSA bone infection by inhibiting pathogen adhesion and biofilm formation, Acta Biomater. 117 (2020) 400–417.
[35] W.R. Osório, C. Brito, L.C. Peixoto, A. Garcia, Electrochemical behavior of Zn-rich Zn–Cu peritectic alloys affected by macrosegregation and microstructural array, Electrochim. Acta 76 (2012) 218–228.
[36] M. Sikora-Jasinska, E. Mostaed, A. Mostaed, R. Beanland, D. Mantovani, M. Vedani, Fabrication, mechanical properties and in vitro degradation behavior of newly developed ZnAg alloys for degradable implant applications, Mater. Sci. Eng. C 77 (2017) 1170–1181.
[37] Y. Xie, L. Zhao, Z. Zhang, X. Wang, R. Wang, C. Cui, Fabrication and properties of porous Zn-Ag alloy scaffolds as biodegradable materials, Mater. Chem. Phys. 219 (2018) 433–443.
[38] K.B. Törne, F.A. Khan, A. Örnberg, J. Weissenrieder, Zn-Mg and Zn-Ag degradation mechanism under biologically relevant conditions, Surface Innovations (2017) 1–41.
[39] B. Jia, H. Yang, Y. Han, Z. Zhang, X. Qu, Y. Zhuang, Q. Wu, Y. Zheng, K. Dai, In vitro and in vivo studies of Zn-Mn biodegradable metals designed for orthopedic applications, Acta Biomater. 108 (2020) 358–372.
[40] M. Lolov, N. Djulgerov, S. Gyurov, Study of the peculiarities of the Zn-Mn phase diagram and their effect on the superplastic behavior of fine-grained Zn-Mn alloys, J. Mater. Eng. Perform. 25 (9) (2016) 3838–3844.
[41] P. Sotoudeh Bagha, S. Khaleghpanah, S. Sheibani, M. Khakbiz, A. Zakeri, Characterization of nanostructured biodegradable Zn-Mn alloy synthesized by mechanical alloying, J. Alloys Compd. 735 (2018) 1319–1327.
[42] Z.-Z. Shi, J. Yu, X.-F. Liu, Microalloyed Zn-Mn alloys: from extremely brittle to extraordinarily ductile at room temperature, Mater. Des. 144 (2018) 343–352.
[43] A. Kafri, S. Ovadia, G. Yosafovich-Doitch, E. Aghion, In vivo performances of pure Zn and Zn-Fe alloy as biodegradable implants, J. Mater. Sci. Mater. Med. 29 (7) (2018) 94.
[44] A. Kafri, S. Ovadia, J. Goldman, J. Drelich, E. Aghion, The suitability of Zn–1.3%Fe alloy as a biodegradable implant, Material, Metals 8 (3) (2018) 153–167.
[45] H. Yang, B. Jia, Z. Zhang, X. Qu, G. Li, W. Lin, D. Zhu, K. Dai, Y. Zheng, Alloying design of biodegradable zinc as promising bone implants for load-bearing applications, Nat. Commun. 11 (1) (2020) 401.
[46] W. Yuan, D. Xia, Y. Zheng, X. Liu, S. Wu, B. Li, Y. Han, Z. Jia, D. Zhu, L. Ruan, K. Takashima, Y. Liu, Y. Zhou, Controllable biodegradation and enhanced osseointegration of ZrO2-nanofilm coated Zn-Li alloy: in vitro and in vivo studies, Acta Biomater. 105 (2020) 290–303.
[47] G. Li, H. Yang, Y. Zheng, X.H. Chen, J.A. Yang, D. Zhu, L. Ruan, K. Takashima, Challenges in the use of zinc and its alloys as biodegradable metals: perspective from biomechanical compatibility, Acta Biomater. 97 (2019) 23–45.
[48] Z. Li, Z.-Z. Shi, H.-J. Zhang, H.-F. Li, Y. Feng, L.-N. Wang, Hierarchical microstructure and two-stage corrosion behavior of a high-performance near-eutectic Zn-Li alloy, J. Mater. Sci. Technol. 80 (2021) 50–65.
[49] Z. Li, Z.-Z. Shi, Y. Hao, H.-F. Li, X.-F. Liu, A.A. Volinsky, H.-J. Zhang, L.-N. Wang, High-performance hot-warm rolled Zn-0.8Li alloy with nano-sized metastable precipitates and sub-micron grains for biodegradable stents, J. Mater. Sci. Technol. 35 (11) (2019) 2618–2624.
[50] S. Zhao, C.T. McNamara, P.K. Bowen, N. Verhun, J.P. Braykovich, J. Goldman, J. W. Drelich, Structural characteristics and in vitro biodegradation of a novel Zn-Li alloy prepared by induction melting and hot rolling, Metall. Mater. Trans. 48 (3) (2017) 1204–1215.
[51] A. Gonzalez-Vazquez, J.A. Planell, E. Engel, Extracellular calcium and CaSR drive osteoinduction in mesenchymal stromal cells, Acta Biomater. 10 (6) (2014) 2824–2833.
[52] Y. Wang, X. Yang, Z. Gu, H. Qin, L. Li, J. Liu, X. Yu, In vitro study on the degradation of lithium-doped hydroxyapatite for bone tissue engineering scaffold, Materials science & engineering, C, Materials for biological applications 66 (2016) 185–192.
[53] D. Brazete, P.M.C. Torres, J.C.C. Abrantes, J.M.F. Ferreira, Influence of the Ca/P ratio and cooling rate on the allotropic α↔β-tricalcium phosphate phase transformations, Ceram. Int. 44 (7) (2018) 8249–8256.
[54] Q. Yuan, Y. Huang, D. Liu, M. Chen, Effects of solidification cooling rate on the corrosion resistance of a biodegradable beta-TCP/Mg-Zn-Ca composite, Bioelectrochemistry 124 (2018) 93–104.
[55] M. Yadi, H. Esfahani, M. Sheikhi, M. Mohammadi, CaTiO3/α-TCP coatings on CP-Ti prepared via electrospinning and pulsed laser treatment for in-vitro bone tissue engineering, Surf. Coating. Technol. 401 (2020) 126256.
[56] A. Oryan, S. Alidadi, Reconstruction of radial bone defect in rat by calcium silicate biomaterials, Life Sci. 201 (2018) 45–53.
[57] L. Fiocco, S. Li, M.M. Stevens, E. Bernardo, J.R. Jones, Biocompatibility and bioactivity of porous polymer-derived Ca-Mg silicate ceramics, Acta Biomater. 50 (2017) 56–67.
[58] Z. Li, X. Gu, S. Lou, Y. Zheng, The development of binary Mg-Ca alloys for use as biodegradable materials within bone, Biomaterials 29 (10) (2008) 1329–1344.
[59] H. Pan, G. Qin, Y. Ren, L. Wang, S. Sun, X. Meng, Achieving high strength in indirectly-extruded binary Mg–Ca alloy containing Guinier–Preston zones, J. Alloys Compd. 630 (2015) 272–276.
[60] D.M. Miskovic, K. Pohl, N. Birbilis, K.J. Laws, M. Ferry, Examining the elemental contribution towards the biodegradation of Mg–Zn–Ca ternary metallic glasses, J. Mater. Chem. B 4 (15) (2016) 2679–2690.
[61] S.J. Sun, S.P. Ju, C.C. Yang, K.C. Chang, I.J. Lee, Effects of Strontium incorporation to Mg-Zn-Ca biodegradable bulk metallic glass investigated by molecular dynamics simulation and density functional theory calculation, Sci. Rep. 10 (1) (2020) 2515.
[62] C.-j. Li, H.-f. Sun, X.-w. Li, J.-l. Zhang, W.-b. Fang, Z.-y. Tan, Microstructure, texture and mechanical properties of Mg-3.0Zn-0.2Ca alloys fabricated by extrusion at various temperatures, J. Alloys Compd. 652 (2015) 122–131.
[63] T. Kokubo, H. Takadama, How useful is SBF in predicting in vivo bone bioactivity? Biomaterials 27 (15) (2006) 2907–2915.
[64] X. Liu, H. Yang, P. Xiong, W. Li, H.-H. Huang, Y. Zheng, Comparative studies of Tris-HCl, HEPES and NaHCO3/CO2 buffer systems on the biodegradation behaviour of pure Zn in NaCl and SBF solutions, Corrosion Sci. 157 (2019) 205–219.
[65] M. Geetha, A.K. Singh, R. Asokamani, A.K. Gogia, Ti based biomaterials, the ultimate choice for orthopaedic implants – a review, Prog. Mater. Sci. 54 (3) (2009) 397–425.
[66] P.K. Bowen, E.R. Shearier, S. Zhao, R.J. Guillory 2nd, F. Zhao, J. Goldman, J. W. Drelich, Biodegradable metals for cardiovascular stents: from clinical concerns to recent Zn-alloys, Advanced healthcare materials 5 (10) (2016) 1121–1140.
[67] D. Druecke, S. Langer, E. Lamme, J. Pieper, M. Ugarkovic, H.U. Steinau, H. H. Homann, Neovascularization of poly(ether ester) block-copolymer scaffolds in vivo: long-term investigations using intravital fluorescent microscopy, J. Biomed. Mater. Res. 68 (1) (2004) 10–18.
[68] J. Fu, C. Wiraja, H.B. Muhammad, C. Xu, D.A. Wang, Improvement of endothelial progenitor outgrowth cell (EPOC)-mediated vascularization in gelatin-based hydrogels through pore size manipulation, Acta Biomater. 58 (2017) 225–237.
[69] J. Rouwkema, N.C. Rivron, C.A. van Blitterswijk, Vascularization in tissue engineering, Trends Biotechnol. 26 (8) (2008) 434–441.
[70] R. Huiskes, H. Weinans, B.v. Rietbergen, The relationship between stress shielding and bone resorption around total hip stems and the effects of flexible materials, Clin. Orthop. Relat. Res. 274 (1991) 124–134.
[71] G. Yu, Z. Li, S. Li, Q. Zhang, Y. Hua, H. Liu, X. Zhao, D.T. Dhaidhai, W. Li, X. Wang, The select of internal architecture for porous Ti alloy scaffold: a compromise between mechanical properties and permeability, Mater. Des. 192 (2020) 108754.
[72] X. Wang, Y. Wang, W. Gou, Q. Lu, J. Peng, S. Lu, Role of mesenchymal stem cells in bone regeneration and fracture repair: a review, Int. Orthop. 37 (12) (2013) 2491–2498.

[73] J.R. Lieberman, A. Daluiski, T.A. Einhorn, The role of growth factors in the repair of bone : biology and clinical applications, JBJS 84 (6) (2002).
[74] H. Zhang, X. Jia, F. Han, J. Zhao, Y. Zhao, Y. Fan, X. Yuan, Dual-delivery of VEGF and PDGF by double-layered electrospun membranes for blood vessel regeneration, Biomaterials 34 (9) (2013) 2202–2212.
[75] T.J. Cho, L.C. Gerstenfeld, T.A. Einhorn, Differential temporal expression of members of the transforming growth factor beta superfamily during murine fracture healing, J. Bone Miner. Res. 17 (3) (2002) 513–520.
[76] N.L. Fazzalari, Bone fracture and bone fracture repair, Osteoporos. Int. 22 (6) (2011) 2003–2006.
[77] L. Claes, S. Recknagel, A. Ignatius, Fracture healing under healthy and inflammatory conditions, Nat. Rev. Rheumatol. 8 (3) (2012) 133–143.
[78] H.C. Fayaz, P.V. Giannoudis, M.S. Vrahas, R.M. Smith, C. Moran, H.C. Pape, C. Krettek, J.B. Jupiter, The role of stem cells in fracture healing and nonunion, Int. Orthop. 35 (11) (2011) 1587–1597.
[79] R. Marsell, T.A. Einhorn, The biology of fracture healing, Injury 42 (6) (2011) 551–555.
[80] N.M. Lowe, N.M. Lowe, W.D. Fraser, M.J. Jackson, Is there a potential therapeutic value of copper and zinc for osteoporosis? Proc. Nutr. Soc. 61 (2) (2002) 181–185.
[81] J. Zheng, X. Mao, J. Ling, Q. He, J. Quan, Low serum levels of zinc, copper, and iron as risk factors for osteoporosis: a meta-analysis, Biol. Trace Elem. Res. 160 (1) (2014) 15–23.
[82] M. Yamaguchi, M. Goto, S. Uchiyama, T. Nakagawa, Effect of zinc on gene expression in osteoblastic MC3T3-E1 cells: enhancement of Runx2, OPG, and regucalcin mRNA expressions, Mol. Cell. Biochem. 312 (1–2) (2008) 157–166.
[83] M. Bruderer, R.G. Richards, M. Alini, M.J. Stoddart, Role and regulation of RUNX2 in osteogenesis, Eur. Cell. Mater. 28 (2014) 269–286.
[84] X. Luo, D. Barbieri, N. Davison, Y. Yan, J.D. de Bruijn, H. Yuan, Zinc in calcium phosphate mediates bone induction: in vitro and in vivo model, Acta Biomater. 10 (1) (2014) 477–485.
[85] W. Huang, S. Yang, J. Shao, Y. Li, Signaling and transcriptional regulation in osteoblast commitment and differentiation, Front. Biosci. 12 (2007) 3068–3092.
[86] N.S. Soysa, N. Alles, NF-kappaB functions in osteoclasts, Biochem. Biophys. Res. Commun. 378 (1) (2009) 1–5.
[87] A. Gür, L. Çolpan, K. Nas, R. Çevik, J. Saraç, F. Erdoan, M.Z. Düz, The role of trace minerals in the pathogenesis of postmenopausal osteoporosis and a new effect of calcitonin, J. Bone Miner. Metabol. 20 (1) (2002) 39–43.
[88] J.d. Boer, H.J. Wang, C.v. Blitterswijk, Effects of Wnt signaling on proliferation and differentiation of human mesenchymal stem cells, Tissue Eng. 10 (3) (2004) 393–401.
[89] Z. Zhu, J. Yin, J. Guan, B. Hu, X. Niu, D. Jin, Y. Wang, C. Zhang, Lithium stimulates human bone marrow derived mesenchymal stem cell proliferation through GSK-3beta-dependent beta-catenin/Wnt pathway activation, FEBS J. 281 (23) (2014) 5371–5389.
[90] C. Hartmann, A Wnt canon orchestrating osteoblastogenesis, Trends Cell Biol. 16 (3) (2006) 151–158.
[91] L. Tang, Y. Chen, F. Pei, H. Zhang, Lithium chloride modulates adipogenesis and osteogenesis of human bone marrow-derived mesenchymal stem cells, Cell. Physiol. Biochem. 37 (1) (2015) 143–152.
[92] X. Wang, S. Zhu, X. Jiang, Y. Li, D. Song, J. Hu, Systemic administration of lithium improves distracted bone regeneration in rats, Calcif. Tissue Int. 96 (6) (2015) 534–540.
[93] M.C. Peterson, M.M. Riggs, A physiologically based mathematical model of integrated calcium homeostasis and bone remodeling, (1873-2763 (Electronic)).
[94] M.M. Dvorak, A. Siddiqua, D.T. Ward, D.H. Carter, S.L. Dallas, E.F. Nemeth, D. Riccardi, Physiological changes in extracellular calcium concentration directly control osteoblast function in the absence of calciotropic hormones, Proc. Natl. Acad. Sci. U. S. A. 101 (14) (2004) 5140–5145.
[95] K. Kapoor, M. Pi, S.K. Nishimoto, L.D. Quarles, J. Baudry, J.C. Smith, The carboxylation status of osteocalcin has important consequences for its structure and dynamics, Biochim. Biophys. Acta Gen. Subj. 1865 (3) (2021) 129809.
[96] A.S. Wagner, K. Glenske, V. Wolf, D. Fietz, S. Mazurek, T. Hanke, A. Moritz, S. Arnhold, S. Wenisch, Osteogenic differentiation capacity of human mesenchymal stromal cells in response to extracellular calcium with special regard to connexin 43, Ann. Anat. 209 (2017) 18–24.
[97] A.M. Barradas, H.A. Fernandes, N. Groen, Y.C. Chai, J. Schrooten, J. van de Peppel, J.P. van Leeuwen, C.A. van Blitterswijk, J. de Boer, A calcium-induced signaling cascade leading to osteogenic differentiation of human bone marrow-derived mesenchymal stromal cells, Biomaterials 33 (11) (2012) 3205–3215.
[98] Z. Huang, S.L. Cheng, E. Slatopolsky, Sustained activation of the extracellular signal-regulated kinase pathway is required for extracellular calcium stimulation of human osteoblast proliferation, J. Biol. Chem. 276 (24) (2001) 21351–21358.
[99] I.A. Silver, R.J. Murrills, D.J. Etherington, Microelectrode studies on the acid microenvironment beneath adherent macrophages and osteoclasts, Exp. Cell Res. 175 (2) (1988) 266–276.